Microstructural Change of Clay under Compression

Riqing Xu[1 and 2], Jiaqi Jiang[1 and 2], Yuming Huang[3], and Jianlin Yu[1 and 2]
[1]*Research Center of Coastal and Urban Geotechnical Engineering, Zhejiang University, Hangzhou 310058, Zhejiang, China*
[2]*Engineering Research Center of Urban Underground Development of Zhejiang Province, Hangzhou 310058, Zhejiang, China*
[3]*Housing and Construction Bureau of Shaoxing, Shaoxing 312000, Zhejiang, China*
E-mail: jiangjiaqi@zju.edu.cn

ABSTRACT: Triaxial test and SEM test are combined to investigate the microstructural variation of Zhejiang marine clay during compression. SEM images are processed and analysed quantitatively, employing an improved determination for threshold. Then the concept of critical threshold is proposed. The test results show that: during compression, it was the pores with middle and large size which were mainly compressed. 2D porosity and fractal dimension showed a decreasing trend, indicating that pore morphology tended to be uniform. A linear relationship between 2D porosity and real porosity can be observed. Similarly, a positive correlation was established between real porosity and fractal dimension. No obvious orientation was found for both clay particles and pores. Finally, the ellipticity distribution of clay particles were stable and concentrated in the interval of 0.4~0.6. some of the macroscopic properties, such as isotropy and internal friction angle, can be a reflection of these variations in microstructure.

KEYWORDS: Triaxial compression, SEM, Microstructure, Critical threshold, Quantitative analysis**.**

1. INTRODUCTION

Marine clays are distributed widely along coastal areas in southeastern China. Due to a long-term erosion, marine sediment with a thickness ranging from a few meters to hundreds of meters is accumulated. Some geotechnical properties for different kinds of marine clays such as compression, shear strength and permeability were discussed by many researchers (Miao et al., 2007; Liu et al., 2011; Jiang et al., 2013; Zhao et al., 2018).

Zhejiang, located in the region of Yangtze river delta, is one of the relatively developed areas in China. More recently, with the increase in civil engineering construction in this area, it's urgently required to sufficiently investigate the engineering behaviours of the Zhejiang marine clay, especially in fields of ground treatment, underground space development and offshore oil exploration. Besides the factors such as sedimentary environment, geophysical characteristics, geological structure and clay minerals, a variety of studies have argued the significant impact of microstructure on the engineering properties (Tanaka & Locat, 1999; Low et al., 2008; Gong et al., 2009; Jiang et al., 2009; Delage, 2010; Yin et al., 2011; Yi et al., 2015; Chen et al., 2019).

As early as 1925 the concept of microstructure in the soil was proposed Terzaghi. For a long period since that, little progress was made in this area due to the lack of reliable experimental technique. Researches on the microstructure in soil has been widely carried out since 1990s, benefiting from the advance in test technology. At present, a variety of techniques including X-ray diffraction (Theisen & Bellis, 1964; Gnanapragasam et al., 1995; Sleutel et al., 2008; Ma et al., 2015), scanning electron microscopy (Jang & Frost, 2000; Li, 2019), mercury intrusion porosimetry (MIP) (Delage et al., 1996; Sasanian & Newson, 2013; Rao & Acharya, 2017) are available. The focus of each technique differs, for example, the X-ray is mostly used for the analysis of the mineralogical change in soil, while the information on the distribution of pores within the clay can be quantitatively measured by MIP. With SEM test, also performed in this research, quantitative data about size and shape of clay particles can be obtained employing graphical analysis.

In this paper, the quantitative analysis of microstructural variation in marine clay during compression is done using SEM technique. With the assistant of graphic processing technology, the relevant microstructure data are extracted. Finally, some indices in the literature are employed to quantitatively describe the changes in microstructure.

2. LABORATORY TESTING

2.1 Soil Description

The soft soils in coastal regions of Zhejiang are mainly composed of silty clay, clay, muddy clay and mud. The clayey silt and sandy soils are relatively less. Their engineering properties are generally characterized by large compressibility, low bearing capacity and permeability, due to its high water content and large void ratio. More than this, the properties of Zhejiang marine clays are usually variable from site to site and with depth. According to the test results of Xu et al. (2012) and Hu et al. (2018), the water content in this region ranges from 20% ~ 90%, especially for some mud, whose value is up to 96.2%. and the plasticity index I_p, defined as the difference of liquid limit w_l and plastic limit w_p, varies from 8~30, increasing with the clay content. The permeability coefficient is generally between 1.0×10^{-9} m/s and 1.0×10^{-7} m/s, and the compression modulus E_s is about 1.5MPa ~ 5MPa, with the minimum for mud which is only about 1.1MPa.

The samples used in this study are taken from two different sites in Zhejiang: Hangzhou and Taizhou respectively. As shown in Figure 1, Hangzhou is located in the northeastern of Zhejiang Province, west of Hangzhou Bay. Due to long-term geological effects, a large amount of grayish yellow and grayish black muddy clay has been deposited. Taizhou is located in the eastern of Zhejiang Province. There are many mountains in the west of Taizhou, in contrast to the plains in the middle and east, so the terrain is higher in the west. As a result, the sediments in this area are mostly mud and muddy clay. The basic physical properties of the soil samples in two sites are shown in Table 1.

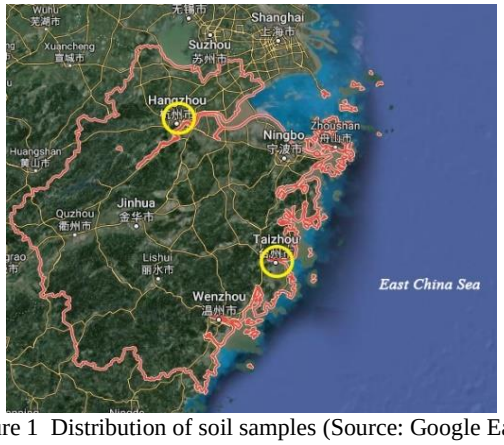

Figure 1 Distribution of soil samples (Source: Google Earth)

Table 1 Physical properties of soil samples

Site	Unit weight (kN/m^3)	Water content w (%)	Specific gravity G_s	Liquid limit w_l (%)	Plastic limit w_p (%)	I_p
Hangzhou	20.1	30.1	2.71	45.9	21.4	24.5
Taizhou	18.6	42.7	2.73	45.6	24.7	20.9

2.2 Sample Preparation and Test Scheme

In this test, the remodeled samples were adopted in consideration of the following factors:

- undisturbed samples are not available for muddy clay in Taizhou due to its high water content
- to ensure the consistency of the initial state for all specimen
- the purpose of this test is focus on the varying process of the microstructure during compression deformation. Therefore, it is not required whether the sample is disturbed or not.

Sample preparation followed the Chinese standard for soil test method (GB/T50123-1999). The original samples were dried and crushed into fine powder that could pass through a 2-mm sieve. Then the screened samples were sealed and preserved. All the tests were done on 39.1-mm-diameter and 80-mm-high specimens which were carefully compacted in four layers from the soil samples. Here, the height of each layer was controlled at about 2cm, following some other practice in literature (Wichtmann et al., 2019). Initial void ratio of all specimens was controlled at about 0.89. Triaxial tests were carried out with the GDS triaxial system (GDSTTS) at Zhejiang University.

Two series of conventional triaxial tests were carried out for two different soils, respectively. 3~4 specimens with different degree of compression (denoted by axial strain) were tested for each group. The test scheme in detail can refer to Table 2. The well-prepared specimens were then placed in a vacuum device for saturation. Drained triaxial (consolidation drainage) tests were applied. Before that, a back pressure of 300kPa was employed for back saturation. A B-check was performed subsequently to make sure that B value reaches 0.98 or more. Then consolidation can be carried out, and the compression is controlled by axial displacement whose loading rate is 0.0075 mm /min.

Table 2 Test scheme

Site	Test number	Initial void ratio e_0	Cell pressure (kPa)	Axial strain ε_1 (%)
Hangzhou	HZ-1	0.87	150	4.5
	HZ-2			9
	HZ-3			15
Taizhou	TZ-1	0.91	100	0 (only consolidation)
	TZ-2			5
	TZ-3			11
	TZ-4			17

2.3 Test Results

Figures 2 and 3 show the stress-strain relationship (q-ε_1 curves) and the volumetric strain-axial strain relationship (ε_v-ε_1 curves) of the CD tests. It can be clearly seen that the deformation of 2 types of soils are featured by hardening and shrinkage. In addition, the parallel specimens with distinct degrees of deformation for each group exhibited nearly identical results, indicating the test results are stable and reliable. The peak strength for Hangzhou clay (cell pressure 150 kPa) and Taizhou clay (cell pressure 100 kPa) are 300 kPa and 180 kPa, respectively.

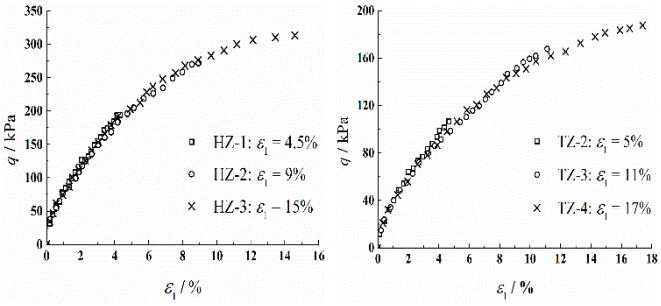

(a) Hangzhou (b) Taizhou

Figure 2 Stress-strain relationship of triaxial compression

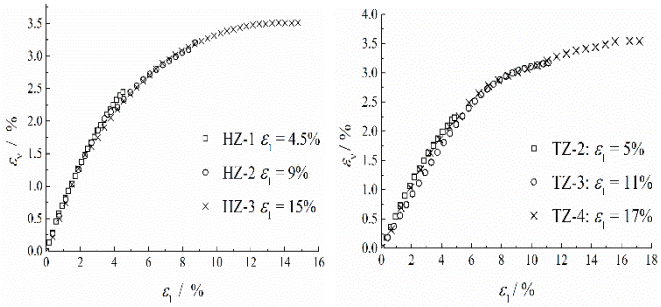

(a) Hangzhou (b) Taizhou

Figure 3 ε_v-ε_1 relationship of triaxial compression

3. QUANTITATIVE INDICES FOR MICROSTRUCTURE OF CLAY AND THE CRITICAL THRESHOLD

As mentioned above, to quantitatively describe the characteristics of microstructure, it is necessary to specify some quantitative indices. In the existing literature, the indicators that can be found about the microstructure of clay mainly involve the following aspects: size, morphology and orientation.

IPP (Image-Pro Plus), an image processing software, has been widely applied in the analysis of microstructural images in the fields of medicine and biology. Recent years, it was gradually introduced into the area of geotechnical analysis (You et al., 2017; Tao et al., 2019; Han et al., 2019). In this study, IPP was used to extract relevant parameters of microscopic image of clay. Based on that, the quantitative indices were calculated.

3.1 Critical Threshold

The first step in graphical analysis of microstructure is to determine the threshold, which is used to converse the grayscale images into the binary figures including only voids and solid particles. There is no unified method for determining the threshold, the common practice in choosing threshold is empirical based. Tang et al. (2008) once suggested that the reasonable threshold of pore structure is 60~100, and for particles 150~220 is acceptable. In this section, the concept of critical threshold is introduced firstly based on the fractal theory.

The fractal theory was first proposed by Mandelbrot (1982) to describe the geometric features of irregular graphics. One important concept in fractal is the self-similarity, which means the local features of structures is similar to that of the entirety in nature. The fractal dimension was first introduced into the analysis of soil microstructure by Moore and Donaldson (1995). Based on their findings, the fractal dimension of the soil can be defined as:

$$LogP = \frac{D}{2} LogA + C \tag{1}$$

where A is the area of soil cluster and P is the corresponding perimeter; D is the fractal dimension and C is an intercept. In this way, fractal dimension is determined by taking the slope of the log-log plot of perimeter against area. It should be noticed that the microstructural indices discussed here (including the fractal dimension) are designed for a certain assembly of soil particles. For a single particle or cluster,

such indices are of little significance. In other words, the microscopic indicators in this research are the average of the soil particle characteristics in the sense of macroscopic statistics.

For a specific SEM image of soil microstructure (See Figure 4(a)), its threshold varies from 0 to 255. Different thresholds are used to binarize the image obtain a division of voids and particles. In Figure 4(b), the part outlined by red line represents the pore structure at a certain threshold. Then the total area and perimeter of all voids (or particles) under each threshold are plotted based on Eq.1 in double logarithmic coordinate, as shown in Figures 4(c) and (d).

It is clear that a linearity both for pore structures and particles exists between the perimeter and area when threshold is relatively small (or large). As the threshold increases, this relationship gradually deviates from linearity, a limit threshold can be found, within which the fractal characteristics of the pore structure (particles) will be maintained. This limit threshold can be defined as the critical threshold, as indicated in the Figure 4. To some extent, the above characteristic is also a manifestation of self-similarity according to the fractal theory. For pores, when below the critical threshold, area identified by IPP is a subset of the real pore structures. Once the threshold exceeds, some particles are mistakenly viewed as pores, so that the fractal feature is broken, and deviation occurs. Therefore, the critical threshold is suggested to distinguish between pores and particles. Generally speaking, the critical thresholds for pores and particles are different. According to the experimental data in this paper, the critical threshold for pores ranges from 70~85, while 180~200 is suitable for particles. This result is basically consistent with the recommendations of Tang et al.

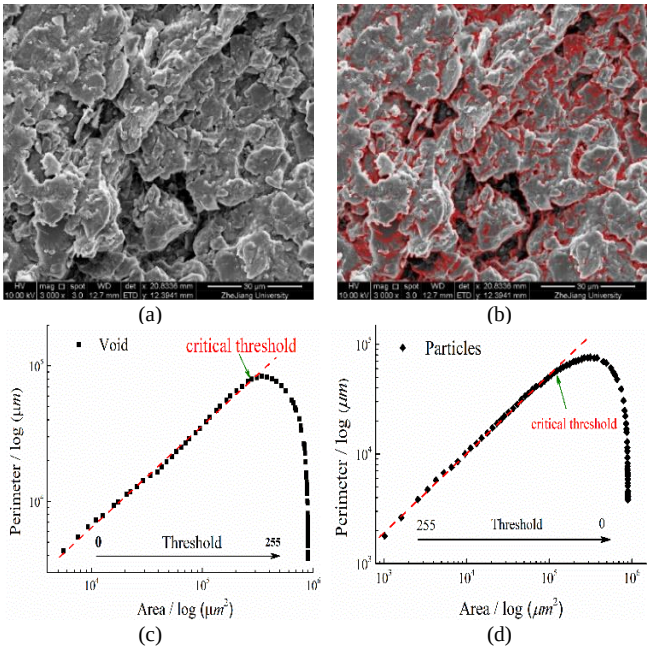

Figure 4 Perimeter-area relationship of void/particle in SEM image with different thresholds

It is easy to point out there is still a very large threshold interval between the above two critical thresholds. For this part, we can interpret as follows: the SEM image is formed by projecting the three-dimensional soil structure onto a two-dimensional plane. Due to the overlap and occlusion between pores and particles, this process is slightly blurred at the interface. In these regions, it's difficult to recognize whether it is counted as a pore or a particle so that the boundary surface is not so clear. To avoid errors caused by these factors, the above method is employed to determine the critical threshold for pores and particles in the discussion of microstructural features.

3.2 Microstructural Indices

As the threshold is determined, the relevant SEM image information can be extracted and calculated to obtain the quantitative indices. Several common indices employed in this paper are:

Fractal dimension, which is widely used in the evaluation of soil microstructure (Malekani et al., 1996; Millan et al., 2007; Wang et al., 2012; Chen et al., 2013; Ghanbarian & Daigle, 2015). As mentioned in the previous section, it's an index that describes the irregularity of the soil structure. At the critical threshold, the perimeter against area of all voids (or particles) are plotted in double logarithmic coordinate (illustrated in Figure 5), and the slope i.e. fractal dimension can be fitted.

2D Porosity, which is defined as the ratio of porous area and total area in SEM image (Zhang et al., 2004). However, the 2D porosity is usually smaller than the real one because part of the pores will be blocked by particles due to the adoption of critical threshold.

Ellipticity, defined as the ratio between major axis and minor axis, representing the degree of flatness of a particle (Shi et al., 1995). It ranges from 0 to 1. For a strip particle, its value closes to 0. In contrast, if ellipticity is close to 1, the shape of a particle is close to a circle.

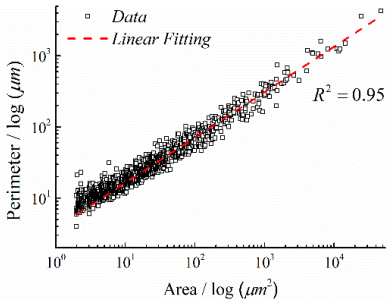

Figure 5 Linear fitting of pore fractal dimension

Alignment entropy *H*, is quantitative index reflecting the extent of order and orientation of the soil fabric, can be calculated via (Mahfouz et al., 2007):

$$H = -\sum_{i=1}^{n} P_i Log_n P_i \tag{2}$$

where all the particles will be divided into *n* groups according to its orientation. *Pi* is the probability that fabric units are located in a certain orientation group. In this study, *n*=18. *H* is also a quantitative index within [0,1]. If all the particles are aligned in a certain orientation group, i.e. *H*=0; and if all particles are arranged in disorder, *H*=1. Alignment entropy is a useful tool to investigate the degree of anisotropy.

4. SEM TEST AND IMAGE PREPROCESSING

After the triaxial tests, soil slices of approximately $10mm \times 10mm \times 5mm$ were cut off from the middle part of the specimens. After air drying the disturbed particles on the surface were blown off to obtain a representative structural cross-section. Then the samples should be taken into the vacuum evaporation coating instrument for gold-plated film to enhance the conductivity of clay. For each specimen, two slices are required, and 2~3 points were selected on each slice for observation and photography. During whole process, effort was made to avoid any structural deformation of the soil and disturbance. SEM tests with Quanta FEG 650 was adapted to scan samples spot by spot.

4.1 Acquisition of Microstructural Image

Figure 6 exhibits the microscopic SEM images of Taizhou clay. As suggested by Tang et al. (2008), magnification of 1000 and 1500 were utilized here because excessive magnification can lead to the "distortion" when focusing on a local region. Larger magnification can be used for auxiliary analysis. Qualitatively speaking, microstructure of Taizhou clay is composed of a sheet-like structure, by which particles and agglomerates connected with each other through face-face, line-face contact. It seems that no obvious orientation could be observed. When comparing Figures 6(a)-(d), it can be observed that as the axial strain increased, the soil showed a

tendency to become dense, at the same time, the number of identifiable particles reduced.

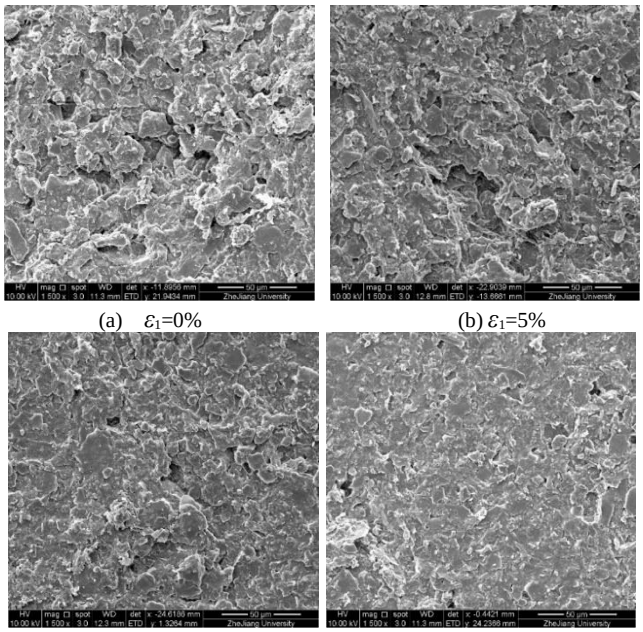

(a) ε_1=0% (b) ε_1=5%

(c) ε_1=11% (d) ε_1=17%

Figure 6 SEM images with different axial strain

4.2 Image Preprocessing

Before extracting the microstructural parameters from SEM image, a necessary preprocessing was performed on the original image, which including image enhancement and denoising. In this experiment, this process is implemented with MATLAB. Image enhancement aims at improve the resolution of the image, and denoising is to remove the interference caused by the instrument and the external environment during the imaging process.

5. QUANTITATIVE EVALUATION ON VARIATION OF MICROSTRUCTURE

5.1 2D Porosity

The size and distribution of pores have a significant effect on the behavior of soft clay. Figure 7 shows the variation of 2D porosity against the axial strain. A negative correlation exists between the 2D porosity and the axial strain, the 2D porosity gradually decreases as the development of axial strain, but the trend gradually slows down. A possible interpretation for this could be that since the axial deformation is uniformly controlled, in the initial stage of deformation, the volume deformation develops fast so that the 2D porosity decreases rapidly. On the other hand, when the deformation reaches a certain level, the volume change will gradually slow down, and the obvious swelling could be observed in the middle part of the specimen, which will result in an increase in porosity. Under the combination of the above two factors, the rate of decrease in 2D porosity slows down.

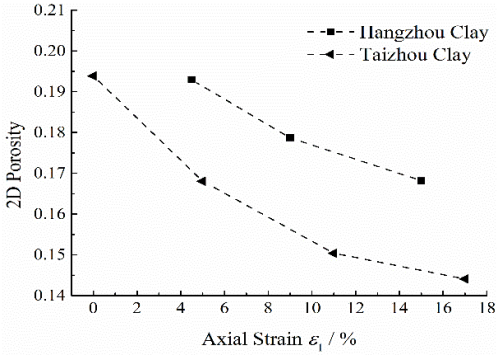

Figure 7 Variation of 2D porosity on axial strain

Figure 8 shows the transformation of distribution in pore size of Hangzhou clay during compression. It can be seen that the pore diameter concentrates on the interval less than 2μm, which accounts for nearly 70%, indicating that the pores structure is mainly composed of tiny and medium pores, and the large pores are relatively less distributed. As the deformation develops, the large-sized pores are obviously compressed and its content reduced; and the corresponding the content of small-sized pores increased. For this, we know that the deformation of saturated soil is a process in which pore water is discharged and the pores are compressed. Compared with small-sized pores, large-sized pores seem much easier to be compressed. When the large-sized pores drop significantly, the compressibility of the soil decreases and the corresponding stiffness is significantly enhanced.

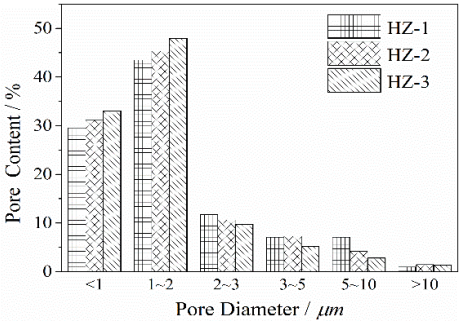

Figure 8 Variation in distribution of pore size

The volume change of soil during the triaxial compression can be directly read, combined with the initial porosity n_0 and volumetric strain ε_v which are known, the void ratio n at any time can be obtained by:

$$n = \frac{n_0 - \varepsilon_v}{1 - \varepsilon_v} \tag{3}$$

Figure 9 shows the relationship between the 2D porosity and the real porosity derived from Eq.3. The 2D porosity determined by SEM graphic analysis differs from the real porosity due to the critical threshold employed here. As previously analyzed, the adoption of critical threshold could make part of pores blocked by particles out of consideration. Despite this, the reliability in analyzing the morphology and orientation of pores/particles can be ensured. Meanwhile, a positive correlation between the 2D porosity and real porosity can be found in Figure 9, which means that the 2D porosity can also reflect the real porosity to some extent.

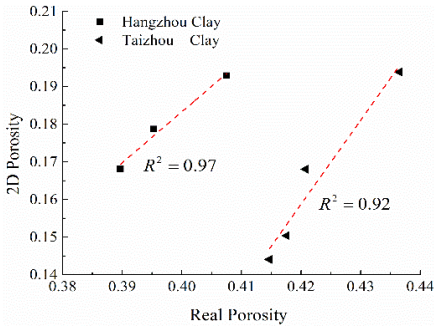

Figure 9 Variation of 2D porosity on real porosity

5.2 Fractal Dimension

The variation of pore fractal dimension on axial strain and real porosity are depicted in Figure 10 and Figure 11, respectively. A similar reduction of pore fractal dimension can be observed as axial strain develops. According to the definition of the fractal dimension, which reflects the complexity of the pore geometry. A higher fractal dimension means that the geometry is more complex. The decrease of pore fractal dimension in this research indicated that the shape of pores tends to be simplified during the compaction.

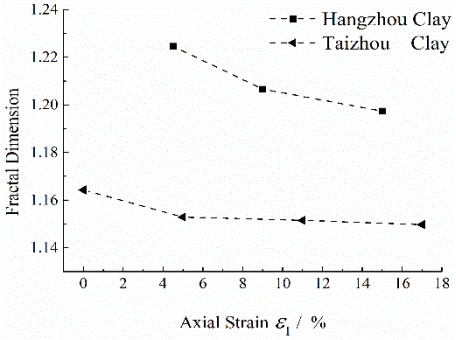

Figure 10 Variation of fractal dimension on axial strain

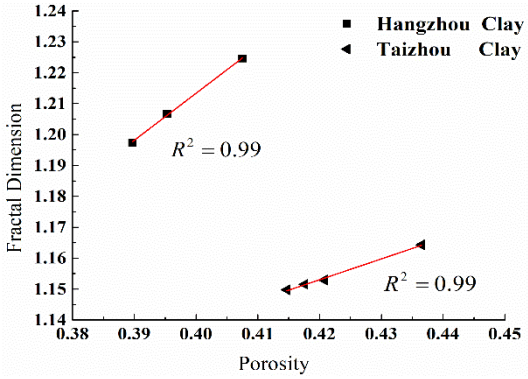

Figure 11 Variation of fractal dimension on porosity

As depicted in Figure 11, there is an approximate linear relationship between the fractal dimension and porosity. For clays in this study, this linear relationship is written as:

$$D = 1.52n + 0.61 \quad \text{(Hangzhou Clay)}$$
$$D = 0.68n + 0.87 \quad \text{(Taizhou Clay)} \tag{4}$$

Eq.4 shows that the pore fractal dimension increases with porosity. It's not difficult to understand because pore structure trends to unified in size distribution, resulting in a decrease in pore fractal dimension.

5.3 Orientation and Alignment Entropy

A rose diagram showing the orientated angle distribution of Taizhou clay is given in Figure 12. The angle between the axis with maximum length and the north direction are defined as the direction angle. the semicircle is divided into 18 equal parts, with 10°an interval. the radius represents the frequency that orientated angle falls into this interval. Although the content in some certain intervals is relatively more than the others, the overall distribution is uniform and has no obvious orientation. Even during the compression, there is no significant change in direction. That is to say, the clay is macroscopically isotropic, and compression does not change this property.

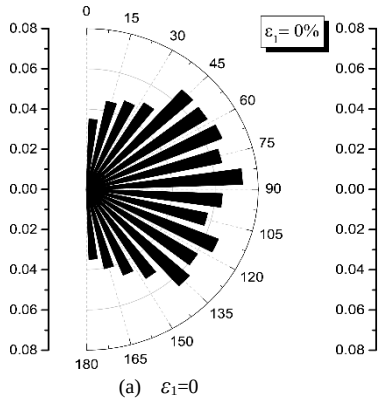

(a) ε_1=0

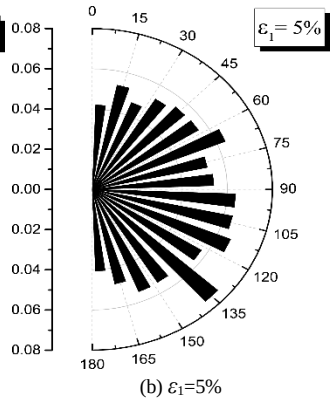

(b) ε_1=5%

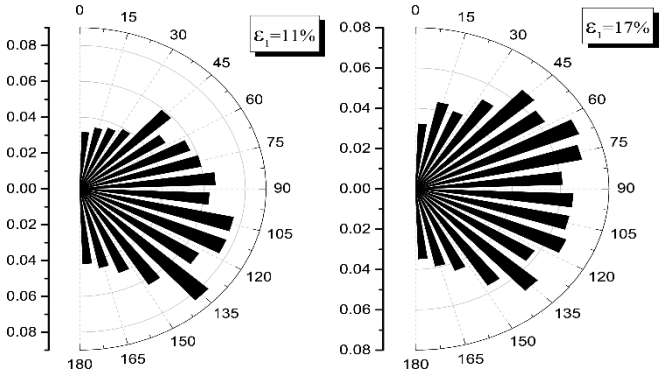

(c) ε_1=11% (d) ε_1=17%

Figure 12 Rose diagram of orientated angle distribution of Taizhou clay with different axial strain

Figure 13 shows the variation of the alignment entropy of particles. The value for both clays has a slight downward, but still maintained above 0.98. Therefore, isotropy is considered reasonable.

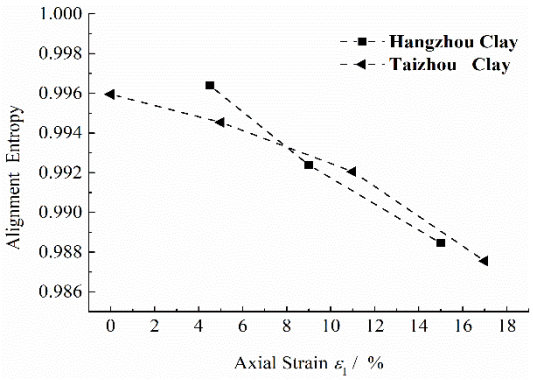

Figure 13 Variation of alignment entropy on axial strain

5.4 Distribution of Ellipticity for Particles

Table 3 gives the distribution of ellipticity of the particles. For both clays, the ellipticity distribution is relatively stable, and there is no obvious change with the deformation. For each soil, the ellipticity is in the range of [0.4, 0.6] is most distributed. That is to say, the particles with aspect ratio about 2:1 is the main component. The content of particles having an ellipticity close to 0 or 1 is very small, in other words, particles with strip-shaped and round shape are very rare. The shape of the particles has a great influence on the frictional strength, internal friction angle in soil mechanics is an important strength index. From the results of this test, the internal friction angle, whose value are 13 degrees and 13.8 degrees for Hangzhou and Taizhou clay, respectively, is basically stable during compression.

Table 3 Ellipticity distribution of soft clay particle

Test number	Ellipticity distribution (%)				
	0~0.2	0.2~0.4	0.4~0.6	0.6~0.8	0.8~1
TZ-1	1.41	25.66	38.44	29.33	5.16
TZ-2	1.49	29.07	39.01	25.57	4.86
TZ-3	1.55	29.70	38.66	24.46	5.63
TZ-4	0.62	24.44	39.86	29.16	5.92
HZ-1	1.30	24.78	41.00	25.30	7.63
HZ-2	0.83	29.51	38.60	24.25	6.81
HZ-3	1.23	26.29	40.84	25.24	6.40

6. CONCLUSION

Quantitative evaluation and analysis were conducted for the microstructural variation under triaxial compression of two representative marine clay in Zhejiang. With the assistant of SEM technology and IPP image process software, some correlation

between microstructure and macroscopic deformation and strength were established. The main findings can be concluded as:

(1) According to the concept of self-similarity in fractal theory, an improved method for threshold determination is proposed, i.e. the so-called critical threshold. Utilizing this threshold, the reliability of SEM image analysis is ensured. However, the downside is that area at the interface of the particles and pores are often underestimated.

(2) The 2D porosity decreases as the develops of axial strain under triaxial compression. An approximate linear correlation was revealed between 2D porosity and real porosity, although they are different in value. During compression, the large-sized pores with diameter greater than 2μm are compressed, and its number reduces significantly. In contrast, the number of pores (diameter less than 2μm) increases, resulting the increase of stiffness.

(3) As the development of axial deformation, fractal dimension of pores gradually decreases, indicating that the pore shape tends to be uniform. Furthermore, there is a certain linear relationship between the pore fractal dimension and real porosity for both clays.

(4) During the deformation, the arrangement of the clay particles is generally disorder, no obvious orientation can be observed. Reflected on the macroscopic level, the clay is isotropic.

(5) The clay particles will gradually bond with each other during the compression. but the distribution of ellipticity of the particles has no significant changes in the whole process, which is mainly concentrated in the interval of [0.4, 0.6]. Macroscopically, it can be understood that the internal friction angle of clay remains stable.

The engineering properties of marine clay are greatly affected by its microscopic fabric. At present, the research on the microstructure of soil is still limited by technical conditions and methods. It is on a stage of preliminary application with very rare practice. The relevant results of this paper can give a better understand for the mechanism of the influence of microstructure on the mechanic properties. However, the soil structure of natural clay has not been considered in this research. Moreover, since the continuous imaging of the microstructure during triaxial compression is difficult to achieve, it was replaced by four parallel specimens with different degrees of deformation. Strictly speaking, the microstructure of the parallel specimens is not exactly the same, but the statistical results of the microscopic indices are reliable provided that the initial conditions of the samples and the loading conditions are consistent.

In the future, with the further development of test technology, more and more advanced measurements will be available. It can be expected that the investigation on microstructure of soil will have a new prospect.

7. ACKNOWLEDGEMENTS

This study was supported by the National Natural Science Foundation of China (Grant No. 41672264) and the Key Research and Development Program of Zhejiang Province (Grant No.2019C03103).

8. REFERENCES

Chen, B., Sun, D. A., and Hu, Y. S. (2019) “Experimental study on strength characteristics and microscopic mechanism of marine soft clays”, Marine Georesources & Geotechnology, DOI: 10.1080/1064119X.2019.1604917.

Chen, H. E., Zhang, J., and Yan, H. (2013) “Quantitative evaluation of microstructure characteristics of cement consolidated soil”, Bulletin of Engineering Geology and the Environment, 72, Issue 2, pp233-236.

Delage, P., Audiguier, M., Cui, Y. I., et al. (1996) “Microstructure of a compacted silt”, Canadian Geotechnical Journal, 33, Issue 1, pp150-158.

Delage, P. (2010) “A microstructure approach to the sensitivity and compressibility of some Eastern Canada sensitive clays”, Geotechnique, 60, Issue 5, pp353-368.

Ghanbarian, B., and Daigle, H. (2015). “Fractal dimension of soil fragment mass-size distribution: A critical analysis”, Geoderma, 245, pp98-103.

Gnanapragasam, N., Lewis, B. A. G., and Finno, R. J. (1995) “Microstructural changes in sand-bentonite soils when exposed to aniline”, Journal of Geotechnical Engineering-ASCE,121, Issue 2, pp119-125.

Gong, S. L., Li, C., and Yang, S. L. (2009) “The microscopic characteristics of Shanghai soft clay and its effect on soil body deformation and land subsidence”, Environmental Geology, 56, Issue 6, pp1051-1056.

Han, B., Lu, G. Y., and Zhu, Z. Q., et al. (2019) “Microstructure features of powdery coal-bearing soil based on the digital image measurement technology and Fractal Theory”, Geotech. Geol. Eng., 37, pp1357-1371.

Hu, J., and Ma, F. H. (2018) “Failure investigation at a collapsed deep open cut slope excavation in soft clay”, Geotech. Geol. Eng., 36, pp665-683.

Jang, D. J., and Frost, J. D. (2000) “Use of image analysis to study the microstructure of a failed sand specimen”, Canadian Geotechnical Journal, 37, Issue 5, pp1141-1149.

Jiang, M. J., Zhang, N., and Liu, J. D. (2013) “Compression behaviors of marine clay for coastal reclamation in Dalian, China”, Proc. International Symposium on Coastal Engineering Geology (ISCEG), Shanghai, pp.123-129.

Jiang, M. J., Peng, L. C., and Zhu, H. H., et al. (2009) “Macro- and micro- properties of two natural marine clays in China”, China Ocean Engineering, 23, Issue 2, pp329-344.

Li, J. (2019) “Scanning Electron Microscopy Testing Technology in Geotechnical Engineering”, Acta Microscopica, 28, Issue 3, pp577-585.

Liu, S. Y., Shao, G. H., and Du, Y. J., et al. (2011) “Depositional and geotechnical properties of marine clays in Lianyungang, China”, Engineering Geology, 121, Issues 1-2, pp66-74.

Low, H. E., Phoon, K. K., and Tan, T. S., et al. (2008) “Effect of soil microstructure on the compressibility of natural Singapore marine clay”, Canadian Geotechnical Journal, 45, Issue 2, pp161-176.

Ma, R. M., Cai, C. F., and Li, Z. X., et al. (2015) “Evaluation of soil aggregate microstructure and stability under wetting and drying cycles in two Ultisols using synchrotron-based X-ray micro-computed tomography”, Soil & Tillage Research, 149, pp1-11.

Mahfouz, A. H., Liu, H. L., and Gao, Y. F., et al. (2007) “Microstructure study of soft clayey soil under consolidation by vacuum preloading method”, Geomechanics and Geoengineering, 2, Issue 2, pp97-108.

Malekani, K., Rice, J. A., and Lin, J. S. (1996) “Comparison of techniques for determining the fractal dimensions of clay minerals”, Clays and Clay Minerals, 44, Issue 5, pp677-685.

Mandelbrot, B. B., (1982) “The fractal geometry of nature”, W. H. Freeman, San Francisco.

Miao, L. C., Zhang, J. H., and Chen, Y. N. (2007) “Study on compressibility of Jiangsu marine clay”, Chinese Journal of Geotechnical Engineering, 29, Issue 11, pp1711-1714(in Chinese).

Millan, H., Gonzalez-Posada, M., and Morilla, A. A., et al. (2007) “Self-similar organization of Vertisol microstructure: A pore-solid fractal interpretation”, Geoderma, 138, Issues 3-4, pp185-190.

Moore, C. A., and Donalson, C. F. (1995) “Quantifying soil microstructure using fractals”, Geotechnique, 45, Issue 1, pp105-116.

Rao, S. M., and Acharya, I. P. (2017) “Mercury intrusion porosimetry studies with geopolymers”. Indian Geotechnical Journal, 45, Issue 4, pp495-502.

Sasanian, S., and Newson, T. A. (2013) “Use of mercury intrusion porosimetry for microstructural investigation of reconstituted clays at high water contents”, Engineering Geology, 158, pp15-22.

Shi, B., Li, S. G., and Tolkachev, M. (1995) “Quantitative approach on SEM images of microstructure of clay soils”, Science in China Series B-Chemistry Life Sciences & Earth Sciences, 38, Issue 6, pp741-748.

Sleutel, S., Cnudde, V., and Masschaele, B., et al. (2008) "Comparison of different nano- and micro- focus X-ray computed tomography set-ups for the visualization of the soil microstructure and soil organic matter", Computers & Geosciences, 34, Issue 8, pp931-938.

Tanaka, H., and Locat, J. (1999) "A microstructural investigation of Osaka Bay clay: the impact of microfossils on its mechanical behavior", Canadian Geotechnical Journal, 36, Issue 3, pp493-508.

Tang, C. S., Shi, B., and Wang, B. J. (2008) "Factors affecting analysis of soil microstructure using SEM", Chinese Journal of Geotechnical Engineering, 30, Issue 4, pp560-565(in Chinese).

Tao, G. L., Peng, W., and Xiao, H. L., et al. (2019) "Numerical simulation and microscopic Stress mechanism for the microscopic pore deformation during soil compression", Advances in Civil Engineering, DOI: 10.1155/2019/ 1542797.

Theisen, A. A., and Bellis, E. (1964) "Quantitative analysis of clay mineral mixtures by X-ray diffraction", Nature, 204, Issue 496, pp1228-1230.

Wang, H. M., Liu, Y., and Song, Y. C., et al. (2012) "Fractal analysis and its impact factors on pore structure of artificial cores based on the images obtained using magnetic resonance imaging", Journal of Applied Geophysics, 86, pp70-81.

Wichtmann, T., Triantafyllidis, Th., and Spath, L. (2019) "On the influence of grain shape on the cumulative deformations in sand under drained high-cyclic loading", Soils and Foundations, 59, Issue 1, pp208-227.

Xu, Y. Q., Li, P. E., and Li, P., et al. (2012) "Physical and mechanical properties of fine-grained soil in the Zhejiang-Fujian coastal area, China", Marine Georesources and Geotechnology, 30, pp130-142.

Yin, Z. Y., Hattab, M., and Hicher, P. Y. (2011) "Multiscale modeling of a sensitive marine clay", International Journal for Numerical and Analytical Methods in Geomechanics, 35, Issue 15, pp1682-1702.

Yi, Y. L., Gu, L. Y., and Liu, S. Y. (2015) "Microstructural and mechanical properties of marine soft clay stabilized by lime-activated ground granulated blastfurnace slag", Applied Clay Science,103, pp71-76.

You, Z. M., Lai, Y. M., and Zhang, M. Y., et al. (2017) "Quantitative analysis for the effect of microstructure on the mechanical strength of frozen silty clay with different contents of sodium sulfate", Environ Earth Sci, 76, Issue 4, pp143.

Zhang, J. R., Liu, Y. Z., and Liu, Z. D. (2004) "Quantitative analysis of micro-porosity of eco-material by using SEM technique", Journal of Wuhan University of Technology-Materials Science Edition, 19, Issue 2, pp35-37.

Zhao, Y., Du, X. L., and Xiong, B. L., et al. (2018) "Experimental study on dynamic characteristics of marine soft clay in North China", Journal of Coastal Research, 83, pp474-478.